Spring 4-30-2015

Investigation of the Lipid Dependence of Respiratory Complex IV Activation Using Nanoscale Bilayers

Matthew Greenwood
University Scholar Program, matthew.greenwood@uconn.edu

INVESTIGATION OF THE LIPID DEPENDENCE OF RESPIRATORY COMPLEX IV ACTIVATION USING NANOSCALE BILAYERS

Matthew Ryan Greenwood

Molecular & Cell Biology, Physiology & Neurobiology

ACKNOWLEDGEMENTS:

I would like to thank Dr. Nathan Alder for providing me the opportunity to work in his laboratory, for allowing me to extend my learning far beyond the classroom and work on the single most rewarding project of my undergraduate career. This project has challenged me in so many ways and taught me lessons not listed on any syllabus. I truly appreciate all of your guidance and support over the past three years, and I count myself lucky to have had you as a mentor. I would also like to thank Dr. Victoria Robinson and Dr. Anastasios Tzingounis for their support as members of my University Scholar Committee. I am lucky to have had you as both advisors and professors.

I would like to thank my sister, Victoria Greenwood, for introducing me to the Alder lab, and for being a fantastic guide. Much of what I have achieved today would not have been possible without Victoria's advice and support over the years, and for this, I am immensely grateful.

I would like to thank Modi Sathappa for all of his help and support with the project; from engineering the affinity tag onto Complex IV, to answering every single question that I had. I appreciate how you treated me as a partner as we worked two separate arms of the same project. I would like to thank Ketan Malhotra for his hospitality and willingness to help with any problem that I may have had, even if it delayed his own work. I would like to thank Dr. Christine Schwall and Dr. Judith Landin for being amazing teachers and for their patience while I developed my finesse with laboratory techniques. I would like to thank the other members of the Alder Lab: Sally Chamberland, Melissa Skoryk, and Adrian Coscia, as well as previous members: Maggie Mayer, Ashley Long, and Catie O'Brien, as it has been a pleasure working alongside all of you. I would like to thank all members of the Alder Lab for being so wonderful and being my family on campus. I will never forget my days spent in the lab.

I would like to thank my family and girlfriend for all of the support, as well as for their flexibility and understanding when I had to change plans or work later than expected.

I would like to thank the UConn Honors Program, the UConn Office of Undergraduate Research, and the UConn University Scholar Program for providing me with the means to take advantage of the absolutely fantastic opportunities at UConn. I would like to extend a special thank you to Dr. Monica van Beusekom, Dr. Caroline McGuire, Jodi Eskin, and Dr. Jennifer Lease Butts for making these opportunities possible.

ABSTRACT:

The mitochondrion's energy-transducing inner membrane is home to the electron transport chain, a meshwork of protein complexes vital to maintaining cellular energy balance. The unique lipid composition of the inner membrane of the mitochondrion includes the dimeric phospholipid, cardiolipin, which is vital for the efficient activity of respiratory Complex IV, the terminal member of the electron transport chain. Previous studies have investigated the protein-lipid interaction between respiratory Complex IV and cardiolipin in detergent micelles and found endogenous cardiolipin molecules, which co-purified with the protein. In this study, respiratory Complex IV was purified and the endogenous cardiolipin molecules were removed with porcine phospholipase A2, before being incorporated into the biologically relevant nanodisc model membrane system. The cardiolipin-free respiratory Complex IV was reconstituted into a controlled lipid environment containing the bilayer favoring phospholipid POPC (1-palmitoyl-2-oleoyl-*sn*-glycero-3-phosphocholine) or a biomimetic mixture of lipids, including POPC, POPE (1-palmitoyl-2-oleoyl-*sn*-glycero-3-phosphoethanolamine) and tetraoleoyl cardiolipin, in molar ratios similar to the lipid environment found in the inner mitochondrial membrane. Using this model system, it has been shown that cardiolipin is vital for the proper activity of respiratory Complex IV. Moreover, this work provides initial evidence that cardiolipin contributes to the activity of Complex IV through the presence bulk lipids that do not directly interface with Complex IV as annular lipids. These findings are significant, as they provide insight into the pathology of diseases associated with mitochondrial lipid remodeling pathways such as Barth Syndrome.

INTRODUCTION:

The mitochondrion is a eukaryotic organelle that is vital to energy transduction in the cell. The biochemical processes associated with oxidative phosphorylation, the citric acid cycle and electron transport chain are both present in the mitochondrion. The unique structure of the mitochondrion (Figure 1) is defined by two unique membranes, which define three separate spaces (1). The energy conserving inner mitochondrial membrane, marked by uniquely shaped cristae, surrounds the mitochondrial matrix, an aqueous compartment that is the site of the citric acid cycle and many other biochemical processes. The lipid composition of the inner mitochondrial membrane is 30-40 percent phosphatidylcholine (PC), 30-40 percent phosphatidylethanolamine (PE), and 15-20 percent cardiolipin (2). The inner mitochondrial membrane also contains other lipids, such as phosphatidylserine, phosphatidylinositol, sterols, and sphingolipids, in much lower molar amounts. The intermembrane space is contained within the inner and outer mitochondrial membranes and is much more acidic than the matrix. The porous outer mitochondrial membrane delineates the organelle from the cytoplasm of the cell.

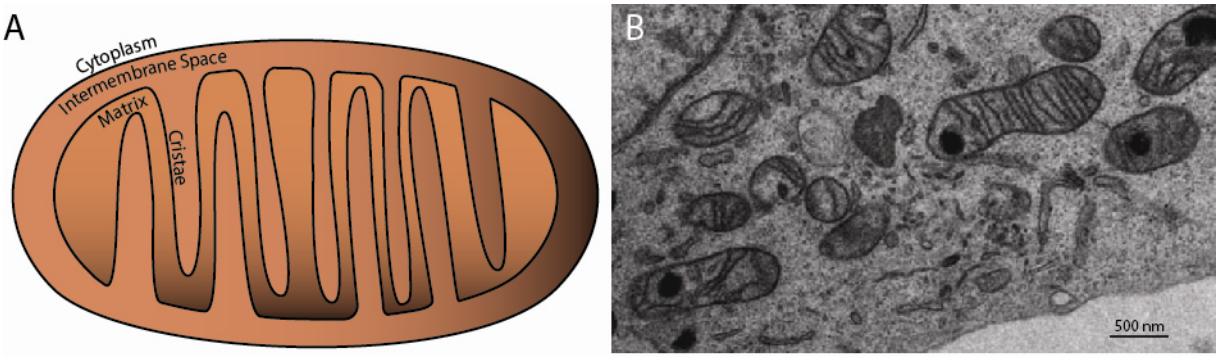

Figure 1 – The Structure of the Mitochondrion
A. A cartoon representation of the mitochondrion **B**. An electron micrograph of mitochondria in HeLa cells. Adapted from Sun et. al.(31).

The mitochondrion is well known for being the powerhouse of the cell, and in addition to maintaining cellular energy balance, is responsible for many vital cellular processes such as the production of precursors to biological macromolecules, the initiation of apoptosis, and the generation of reactive

oxygen species used in cellular signaling pathways (1). The unique structure of the mitochondrion serves to optimize the unique roles that the organelle must carry out for optimal cell function.

The energy generating pathways of the mitochondrion converge on the inner mitochondrial membrane with the electron transport chain (Figure 2). The electron transport chain is fed by NADH and $FADH_2$, electron carriers and products of the citric acid cycle. Electrons supplied to the electron transport chain are shuttled between respiratory complexes via electron carriers, until the electrons are transferred to molecular oxygen. The transfer of electrons between respiratory complexes is coupled with proton pumping from the matrix to the intermembrane space. The highly convoluted nature of cristae, which are enriched in electron transport complexes (3), increases the surface area of the membrane to increase the number of respiratory complexes embedded in the membrane and therefore the amount of ATP that can be generated. The inner mitochondrial membrane has one of the highest protein to lipid ratios observed in nature, with the membrane being composed of approximately 70% protein by weight (2).

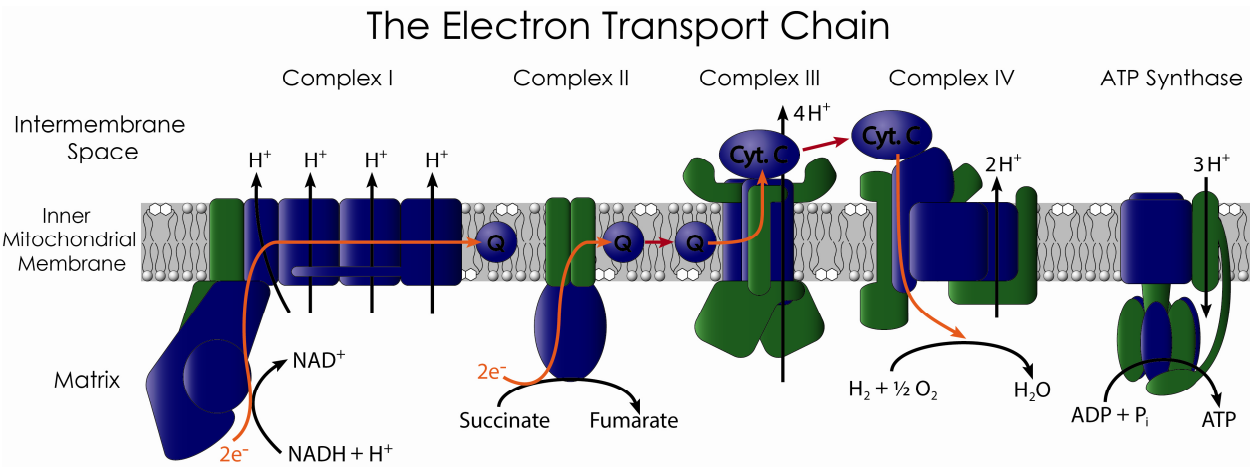

Figure 2 – A Diagram of the Mammalian Electron Transport Chain
Core catalytic subunits of protein complexes are depicted in blue, while regulatory and supernumerary subunits are depicted in green. The flow of electrons is depicted in orange and the movement of protons across the inner mitochondrial membrane is depicted by black arrows. Q represents Coenzyme Q and Cyt. C represents cytochrome *c*.

Electrons from nucleotide electron carriers enter the electron transport chain through Complexes I and II (1). Respiratory Complex I (NADH: ubiquinone oxidoreductate) shuttles electrons from NADH to the quinone Coenzyme Q (Q), a lipid-soluble, hydrophobic electron carrier within the inner mitochondrial membrane. Complex I is found in metazoans, but not in yeast, where instead peripheral NADH dehydrogenases carry out the transfer of electrons from NADH to Q (4). The exergonic flux of electrons from NADH to Q is used to drive four protons across the inner mitochondrial membrane. Respiratory Complex II (Succinate: ubiquinone oxidoreductase) is the only respiratory complex of the electron transport chain that is also a component of the Citric Acid Cycle, which catalyzes the oxidation of succinate to fumarate. The electrons generated by Complex II are used to reduce the quinone pool, just as Complex I does. The redox reactions mediated by Complex II are not sufficiently exergonic to be coupled with proton pumping; however, Complex II is still vital because of the role it plays in catalyzing an intermediate step in the Citric Acid Cycle, and in reducing the Q pool, as described above. If Complex II did not catalyze the oxidation of succinate, the citric acid cycle would halt, as would the regeneration of electron carriers to supply the electron transport chain. Respiratory Complex III (ubiquinone: cytochrome c oxidoreductase) transfers electrons from the QH_2 pool, reduced by Complexes I and II, to cytochrome *c*. The electron transfer carried out by Complex III is unique because QH_2 carries two electrons, whereas cytochrome *c* is only able to carry a single electron. In Complex III, the protein must accept two electrons from Coenzyme Q and individually transfer the electrons to cytochrome *c*. This electron transfer is thermodynamically favorable enough to be coupled with the translocation of four protons across the inner mitochondrial membrane. Cytochrome *c* is a peripheral membrane protein found in the intermembrane space and when released into the cytoplasm, this protein has peroxidase activity and initiates a signal cascade leading to apoptosis. The terminal enzyme of the electron transport chain, respiratory Complex IV (Cytochrome C Oxidase), transfers electrons from cytochrome *c* to molecular oxygen. This reaction produces water and is used to drive two protons

across the inner mitochondrial membrane for every electron transferred from cytochrome *c* (5-7). There are three channels suspected to act as pathways for the movement of protons in Complex IV. Two of the proton channels, known as the D and K channels, shuttle protons needed for the reduction of oxygen (7), while the third proton channel, known as the H channel, is suspected to provide a route for the translocation of protons across the inner mitochondrial membrane (5). Respiratory Complexes I, III, and IV all pump protons across the inner mitochondrial membrane, creating a chemiosmotic gradient across the insulating inner mitochondrial membrane. F_0F_1 ATP Synthase, often referred to as Complex V, harnesses the proton gradient across the membrane to generate ATP from ADP and P_i in a process termed oxidative phosphorylation. F_0F_1 ATP Synthase allows protons to flow down their electrochemical gradient, to drive conformational changes in the catalytic module. Specifically, a protein shaft rotates in ATP Synthase to force the catalytic subunits to adopt specific conformations, which result in the phosphorylation of ADP into ATP.

The inner mitochondrial membrane is enriched with the lipid cardiolipin, the signature phospholipid of energy transducing membranes (8, 9). Cardiolipin is also found bacterial membranes (8, 9); therefore, mitochondrial enrichment of cardiolipin results from the endosymbiotic origin of the organelle. Based on the endosymbiotic theory, the mitochondria found in contemporary eukaryotic cells are derived from an ancestral prokaryote having energy transducing membranes containing cardiolipin (7). Cardiolipin (Figure 3) is a lipid dimer composed of two diacylglycerols that are linked via the phosphate headgroups by a glycerol bridge (9, 10). Cardiolipin contains four acyl chains, in contrast to other phospholipids that contain only two. There is still great debate in the literature over whether or not the pK_a of the phosphates in cardiolipin are identical, or if the two phosphates have disparate pK_a values due to the proposed bicyclic structure of the headgroups stabilized by hydrogen bonds (11, 12).

Cardiolipin is synthesized in the inner mitochondrial membrane through a lipid-remodeling pathway composed of several enzymes (9). Immediately following synthesis, nascent cardiolipin

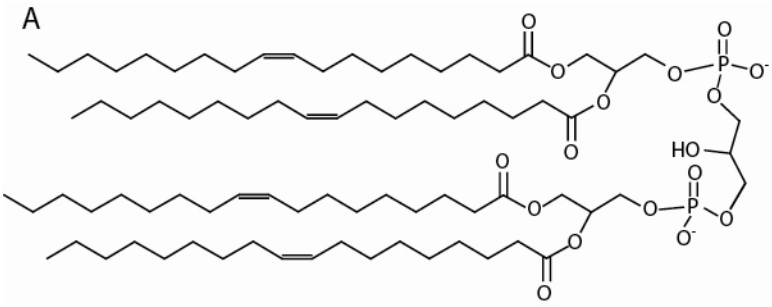

C

	Mitochondria	Endoplasmic reticulum	Lysosomes	Golgi	Plasma membrane
Phospholipid (mg/mg protein)	0.175	0.374	0.156	0.825	0.672
Sterols (mg/mg protein)	0.003	0.014	0.038	0.038	0.128
		% of total phospholipids			
Phosphatidylcholine	44	60	48	51	40
Phosphatidylethanolamine	34	23	17	21	24
Phosphatidylinositol	5	10	6	12	8
Phosphatidylserine	1	2	3	6	9
Cardiolipin	14	1	1	1	1
Phosphatidic acid	<1	1	1	<1	1
Sphingomyelin	1	3	24	8	17
Phosphatidic acid	1	-	-	-	4

Figure 3 – The Structure and Distribution of Cardiolipin
A. The structure of tetraoleoyl cardiolipin. **B.** The structure of the possible bicyclic headgroup of cardiolipin. DAG stands for diacylglycerol. **C.** A table adapted from Horvath and Daum (8) describing the lipid composition of biological membranes found in rat liver.

contains saturated acyl chains and is converted to the mature form when the saturated acyl chains of immature cardiolipin are replaced with unsaturated acyl chains from PE or PC. The final acyl chain profile of mature cardiolipin is tissue-specific in metazoans, and may be related to the energy requirements of the tissue (9). The remodeling process has been well characterized in yeast, where acyl chains on immature cardiolipin are individually cleaved to form monolysocardiolipin, a cardiolipin molecule containing three acyl chains, by cardiolipin deacylase 1 (cld1) (9). The monolysocardiolipin is reacetylated by the tafazzin transacylase enzyme, which transfers acyl chains from donor phospholipids (9). After several rounds of remodeling, all of the saturated acyl chains on immature cardiolipin have been replaced with saturated acyl chains. Cardiolipin has been shown to play both a structural and

catalytic role with several of the respiratory complexes in the electron transport chain, such as Complexes II, III and IV (2, 10, 13, 14). Defects in cardiolipin remodeling can result in a number of pathologies, depending on which component of the remodeling pathway is affected. In Barth syndrome, the cardiolipin remodeling enzyme tafazzin is non-functional and results in gross abnormalities of the mitochondrial lipid profile, including reduced amounts of cardiolipin and increased monolysocardiolipin. Barth syndrome is characterized by a wide range of phenotypes, including cardiomyopathy, neutropenia, growth delay, muscle weakness and exercise intolerance (1, 9, 15). All of these symptoms stem from the reduced efficiency of the mitochondria, underscoring the important role that cardiolipin plays in mitochondrial function. Cardiolipin deficiency in the mitochondrial inner membrane is known to affect the fluidity and stability of the membrane with pronounced effects on the cristae membrane (3).

Borrowing from Jacques Monod's comment on the unifying theme of biochemistry, "anything found to be true of *E. coli* must be true of elephants" (16), respiratory Complex IV has been structurally and functionally well characterized in both mammals, cattle (*Bos tarus*), and fungi, baker's yeast (*Saccharomyces cerevisiae*). While there is high sequence homology between most of the subunits of Complex IV of the two species (5), there are some notable differences between the two holoenzymes; bovine Complex IV is composed of 13 subunits, whereas Complex IV found in yeast is only composed of 11 subunits. Additionally, some isoforms of the accessory subunits of bovine Complex IV are often only expressed in specific tissues, while in yeast isoforms of one subunit are expressed depending on the availability of oxygen for the enzyme (1, 5). As both bovine and yeast Complex IV have been used to study the function Complex IV, it is important to reconcile discrepancies in nomenclature between the two models (Figure 4). For the purpose of clarity, all subunits will be referred to using the yeast nomenclature, unless otherwise stated.

Subunit (subunit length)		Function
Yeast	Bovine	
Cox1 (534)	COX I (514)	Catalytic subunits
Cox2 (236)	COX II (227)	
Cox3 (269)	COX III (261)	
Cox4 (130)	COX Vb (98)	Subunits required for Complex IV assembly and function
Cox5A* (133)	COX IV isoform 1 (147)	
	COX IV isoform 2 (171)	
Cox5B* (134)	COX IV isoform 1 (147)	
	COX IV isoform 2 (171)	
Cox6 (108)	COX Va (109)	
Cox7 (59)	COX VIIa isoform 1 (59)	
	COX VIIa isoform 2 (60)	
Cox8 (47)	COX VIIc (47)	
Cox9 (55)	COX VIc (73)	
-	COX VIIb (56)	
-	COX VIII isoform 1 (44)	
	COX VIII isoform 2 (46)	
Cox12 (82)	COX VIb isoform 1 (85)	Non-essential subunits (possible regulatory function)
	COX VIb isoform 2 (88)	
Cox13 (120)	COX VIa isoform 1 (85)	
	COX VIa isoform 2 (85)	

Figure 4 –Homologous Subunits of Respiratory Complex IV
Cox is an abbreviation of Cytochrome c Oxidase. *Cox5A and 5B are isoforms of the same subunit that are differentially expressed depending on the availability of oxygen. Adapted from the work of Marechal et. al. and Barrientos, et. al. (5, 17)

Respiratory Complex IV is a chimera of protein subunits encoded by both nuclear and mitochondrial DNA. The protein subunits encoded by nuclear DNA accounts for more than 90% of all protein in the mitochondrion by weight (18). Mitochondrial DNA encodes a few highly conserved protein subunits of electron transport complexes, including the three core catalytic subunits of Complex IV, which contain the redox centers essential from function (6, 18). The remaining subunits are encoded by nuclear DNA, translated on cytoplasmic ribosomes and imported into mitochondria, where the subunits are assembled into a complete respiratory complex (1, 5). These subunits either stabilize or assist in the assembly of the complex. Cox1 contains three redox-active metal sites: heme *a*, heme a_3, and a copper ion Cu_B (1, 5). Cox2 contains a binuclear copper site (5). Heme a_3 is the site of oxygen binding and reduction upon electron transfer from cytochrome *c* (1, 6). Cox3 has no redox function, but is involved in the translocation of protons across the inner mitochondrial membrane (1, 6). Electrons transferred from

cytochrome *c* to Complex IV are first donated to Cu_a, then to heme a, before reducing oxygen at heme a_3 and Cu_B (1). Cyanide is a specific inhibitor of Complex IV and binds with extremely high affinity to the complex. Cyanide inserts between heme a_3 and Cu_B (6), inducing a similar conformational change as oxygen upon binding. This prevents the flow of electrons and inhibits the catalytic activity of Complex IV (6).

Respiratory Complex IV exists *in vitro* as a dimer (Figure 5), stabilized by several lipids including four cardiolipin molecules, two per monomer. Some of the cardiolipin molecules bind very tightly to Complex IV and co-purify with the complex (10, 13, 14, 19). Through x-ray crystallography studies, it has been shown that approximately two cardiolipin molecules that co-purify and co-crystalize per Complex IV monomer (6, 10, 14, 20). Numerous studies(14) and computer simulations (21) have shown that cardiolipin molecules interact in two positions per Complex IV; one site is in close proximity to the proton channels of Complex IV, while the other site is composed of bovine subunits VIa and VIb to form dimers of Complex IV (6, 10, 13, 14). The two sets of endogenous cardiolipin molecules bind with differing affinities to Complex IV (14, 22). One pair of low affinity cardiolipin molecules bind at the interface of the monomers and can be removed easily (13, 14, 21, 22). Complex IV is the rate-limiting enzyme of the electron transport chain and is regulated by hormones, lipids, and second messengers (1). In select tissues, a different isoform of bovine Complex IV, subunit VIa is expressed, which allosterically regulates the catalytic activity of the protein depending on the concentration of ATP and ADP (1, 5, 24).

The loss of the weakly associated cardiolipin molecules from the protein complex results in the irreversible dissociation of bovine subunits VIa and VIb and is associated with the dissociation of the Complex IV dimer into monomers (13, 14). This dissociation has not been found to be associated with a loss of enzymatic activity of the protein, as work by Sedlak and Robinson has shown that it was possible to remove subunits VIa and VIb without removing cardiolipin and observed no change in the enzymatic activity (13).

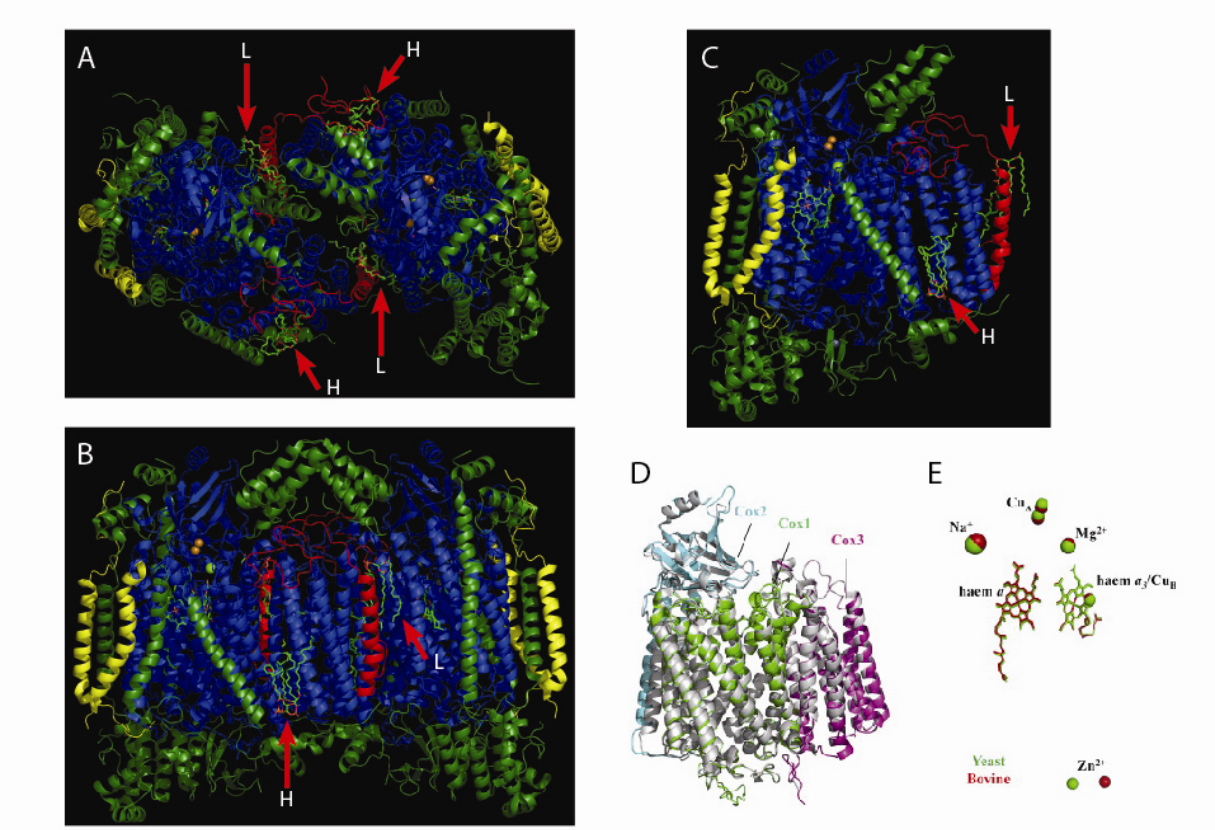

Figure 5 – Crystal Structures of Bovine and Yeast Respiratory Complex IV
Top (**A**) and side (**B**) views of dimeric and monomeric (**C**) bovine respiratory Complex IV co-crystalized with cardiolipin. Endogenous cardiolipin molecules have been labeled with red arrows and identified as having either low (L) or high (H) affinity for Complex IV. The core catalytic subunits have been colored blue, and the accessory subunits have been colored green. Accessory subunits found only in mammals and not in yeast have been colored yellow. COX VIa has been colored red. In **C,** some of the catalytic subunits have been removed to expose the redox metal centers. PDB ID: 2DYR (10) **D.** A superposition of the catalytic core of Bovine (grey) and yeast (colored) Complex IV, showing structural homology. **E.** Superposition of the redox centers found in the catalytic core of bovine and yeast. Figures 5D and 5E were adapted from Marechal et. al.(5) PDB ID: 1V54

The second pair of cardiolipin molecules is tightly bound to Complex IV and is required for the proper activity of the protein (13, 14, 22). To remove the tightly bound cardiolipin molecules, Complex IV must be treated with phospholipase A2, which cleaves cardiolipin at the *sn*-2 position (23). Removal of the tightly bound endogenous cardiolipin molecules results in a 50 percent decrease in the electron transfer activity of the protein complex (5, 9, 13, 22). The tightly bound cardiolipin molecule was found to be located near the entrance to the D proton channel, and is believed to act as a proton antenna for Complex IV (14, 21). If cardiolipin truly has a bicyclic headgroup structure, then cardiolipin could

enhance the catalytic activity of Complex IV by donating protons that are held in the headgroup of the molecule. The decrease in activity associated with phospholipase treatment can be rescued by the addition of exogenous cardiolipin, which recovers more activity than any other lipid (9, 13). Complex IV treated with phospholipase has higher affinity for cardiolipin than any other lipid found in the inner mitochondrial membrane (13).

In addition to stabilizing Complex IV dimers, cardiolipin is known to stabilize other respiratory complexes. Cardiolipin is important for the formation of respiratory supercomplexes, which in yeast, are composed of two monomers of Complex III and one to two monomers of Complex IV (1, 3, 4, 20). Supercomplexes improve the efficiency of oxidative phosphorylation by channeling cytochrome *c* between Complexes III and IV. Substrate channeling improves the efficiency of the transfer of electrons down the electron transport chain because the carriers are able to travel more directly between the different respiratory complexes, rather than relying purely on diffusion for the electron carriers to find the successive respiratory complex (4). Cardiolipin has been shown to improve the formation and stability of supercomplexes containing Respiratory Complexes III and IV (3, 4). In mammals, respiratory supercomplexes can also include Complex I (4, 20). Cardiolipin is believed to be the most important lipid of any respiratory supercomplex because it binds tightly to both Complex III and IV and therefore is believed to play a central role in respiratory supercomplex formation (4). Dissociation of respiratory supercomplexes is the result of decreased levels of cardiolipin and can result in numerous diseases and pathologies (4, 20). A reduction in the abundance of cardiolipin can be caused by oxidative stress from reactive oxygen species in the mitochondrion or by disorders in the cardiolipin remodeling pathway.

The study of membrane proteins provides a technical challenge because membrane proteins are insoluble and have a propensity to aggregate (25, 26). The challenge arises from keeping the protein stable in an aqueous environment. Although several methods have been developed to allow for the study of membrane proteins in an aqueous environment, most of the traditional approaches result in

unstable membrane proteins in an environment that is non-biologically mimetic. One of the most common methods used to study membrane proteins is detergent solubilization. While this method is relatively quick and easy, it places membrane proteins in a micellar, not lamellar environment and can lead to inactivation of the protein over time. Detergent solubilization requires some optimization, as the detergent may denature the protein in question (25, 26). Another drawback to detergent solubilization is that it cannot be used to study protein-lipid interactions. Proteoliposomes are another popular technique employed to study membrane proteins, as this method allows for the study of the protein of interest in a lipid bilayer. This is achieved through the insertion of protein into the membrane of a liposome of defined lipid composition, assuming the lipid blend is able to form stable liposomes. This approach is biologically mimetic and creates an internal and external space that may be taken advantage of experimentally. Although the two discrete compartments can be useful, especially when gradients need to be established, proteoliposomes do not allow easy external access to the internal compartment. Proteoliposomes can be heterogeneously sized, introducing some variation into the experimental system. Additionally, proteoliposomes are large and scatter light, making liposomes poor candidates for use in spectrophotometric studies (25, 26). A relatively novel model membrane system is the nanodisc, a nanoscale lipid bilayer stabilized by an amphipathic protein scaffold into which the protein of interest can be inserted (25, 27). The size of the annular lipid bilayer is determined by the membrane scaffolding protein (MSP) (27), allowing for the creation of a homogenous model membrane system (2). Previous work from our group has shown that the nanodisc model membrane system is able to successfully incorporate mitochondrial membrane proteins (2). Nanodiscs are created using a reaction mixture containing the protein of interest in detergent micelles, membrane scaffolding protein and lipids. Nanodiscs will spontaneously form through the hydrophobic effect when the detergent is removed by adsorbent beads (26). The rate of nanodisc formation is dependent on the temperature and will occur most rapidly when the reaction occurs at a temperature near the melting temperature of the lipids in

the bilayer (26). Nanodiscs are especially useful for the study of protein-lipid interactions as any desired lipid blend that forms a stable bilayer can be used to reconstitute the protein.

In this experiment, I aimed to elucidate the effect that cardiolipin has on the catalytic activity of respiratory Complex IV for the first time in a biologically mimetic model membrane system (Figure 6). This was achieved by purifying respiratory Complex IV out of mitochondria derived from *S. cerevisiae* and removing the endogenous cardiolipin with porcine phospholipase A2. The lipid-free Complex IV was incorporated into the nanodisc model membrane system containing lipid blends in which cardiolipin was either present or absent. The biomimetic (BM) lipid blends contained cardiolipin and were similar to the mitochondrial inner membrane (40 mole % POPC, 40 mole % POPE, and 20 mole % tetraoleoyl cardiolipin). The cardiolipin deficient samples contained only POPC.

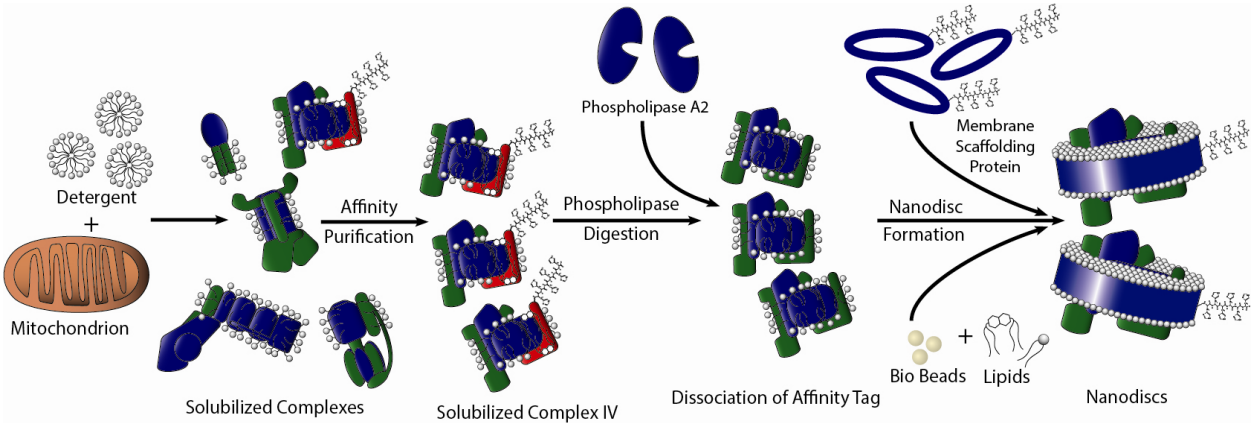

Figure 6 – Experimental Approach
Please note, not all steps are shown. Catalytic subunits of protein complexes are depicted in blue, and regulatory and supernumerary subunits are depicted in green. Red subunits depict mutant Cox13 containing an affinity tag. Following phospholipase treatment, Cox13 dissociates from the protein complex, coinciding with the transition of Complex IV from the dimeric to monomeric state.

Materials & Methods:

Materials

Lipids were purchased form Avanti Polar Lipids (Alabaster, AL). Chemicals were obtained from Sigma Aldrich (St. Louis, MO) or Thermo Fisher Scientific, Inc. (Pittsburg, PA).

Homologous Recombination

Our group engineered a hexahistidine tag onto the carboxyl terminus of Cox13 on respiratory Complex IV of *S. cerevisiae*, strain WT303-1A. The location of Cox13 has been depicted in red in Figures 5A-C. The added affinity tag allows for the efficient purification of respiratory Complex IV via affinity purification on a Ni-NTA column. The hexahistidine tag was combined with the genetic sequence for kanamycin resistance and was targeted to the yeast genome through homologous recombination, as has been previously described (7). Work by Meunier et. al. has shown that engineering an affinity tag onto Complex IV has no effect on the catalytic activity of the protein.

Mitochondria Growth and Preparation

Mitochondria were isolated from *S. cerevisae*, strain WT303-1A*,* engineered to contain an affinity tag on the carboxyl terminus of Cox13. Colonies of *S. cerevisiae* were grown on YEP Lactate + Adenine + Geneticin plates for three days. *S. cerevisiae* was grown from single colonies in successive overnight growth periods in increasing volumes of non-fermentable, undefined media SSLac (2% Na-Lactate, 3 g/L yeast extract, 5.7 mM KH_2PO_4, 18.7 mM NH_4Cl, 8.5 mM NaCl, 4.5 mM $CaCl_2$, 2.9 mM $MgCl_2$~$6H_2O$, 2.7 mM D-(+) glucose, 170 µM Adenine Hemisulfate salt, and 250 µg/mL Geneticin, pH 5.5). First, 5 mL culture tubes of SSLac were inoculated with single colonies and allowed to grow overnight in a 30°C incubator set to 250 RPM. The two cultures with the highest optical density (OD) at 600 nm were transferred to 100 mL cultures and again grown overnight under the same conditions. The following night, the culture with the highest OD was transferred in 15 mL aliquots to each of the five 800 mL cultures and grown overnight. The following morning, the media containing *S. cerevisiae* was centrifuged in 250 mL Beckman bottles in a GSA rotor for 5 minutes at 5,000 RPM. The supernatant was decanted and the pellets of *S. cerevisiae* combined. The combined pellets were resuspended in Buffer

TD (100 mM Tris-SO_4 and 10 mM DTT, pH 9.4), with 1 mL of Buffer TD for every 0.3 grams of pellet and incubated at 30°C for 15 minutes at 100 RPM. The cells were centrifuged for 5 minutes at 5,000 RPM and the supernatant decanted. The pellets were resuspended in Buffer SP (20 mM KPO_4 and 1.2 M sorbitol, pH 7.4) to remove DTT, before being pelleted again. The pellets were resuspended in 1 mg/mL of Zymolase in Buffer SP, with 2 mg of Zymolase for every gram of cells. The cells were incubated at 37°C for 37 minutes at 125 RPM to allow for cell wall digestion. The solutions were tested for the formation of spheroplasts before proceeding. After spheroplast formation, all steps were performed on ice. Spheroplasts were collected by gentle centrifugation at 3.5 RPM for 5 minutes and resuspended in Buffer SP. Resuspension and centrifugation was repeated twice more. The spheroplast pellets are resuspended in S.E.H. Buffer (250 mM sucrose, 20 mM HEPES, 1 mM EDTA, 0.5% BSA, 1 mM PMSF, 1 µg/mL Leupeptin, and 1 µg/mL Aprotinin, pH 7.5). Spheroplast solutions are homogenized with a 15 mL Dounce homogenizer and homogenized with 15 strokes. Following homogenization, the solutions are transferred to 50 mL tubes and centrifuged in a Sorvall SA-600 rotor at 3,500 RPM for 5 minutes. The supernatant (Supernatant A) is transferred to new tubes, while the pellets are resuspended (Supernatant B) and homogenized again. Supernatant B was centrifuged at 3,500 RPM for 5 minutes and the supernatant was then combined with Supernatant A. Combined supernatants were centrifuged at 10,000 RPM for 10 minutes. The resulting pellets were resuspended in 20 mL of S.E.H. Buffer and subjected to two more rounds of slow and fast spins. The final pellets were resuspended in 0.5 mL S.E.H. Buffer. The mitochondrial concentration of the resuspended pellets was determined using ε_{280} of 0.021 mg/mL^{-1} cm^{-1}. Mitochondrial samples were flash frozen in 2 mg aliquots and stored at -80°C until needed.

Reduction of Cytochrome C

Reduced cytochrome *c* from Equine heart was prepared by adding 60 mg of cytochrome *c* to 500 µL of Assay Buffer (50 mM KPO_4 and 50 µM EDTA, pH 7.4). Five mg of Ascorbate was added to reduce cytochrome *c* (28) and was incubated until cytochrome *c* turned from brown to red. The reduced cytochrome *c* was purified using a Sephadex G25 column equilibrated with Assay Buffer. Fractions were collected in 10-drop aliquots and peak fractions were pooled. The concentration of reduced cytochrome *c* was determined with an ε_{550} RED of 27.4 mM^{-1} cm^{-1}.

Transformation of Competent Cells

To produce nanodisc scaffolding protein, competent *Escherichia Coli* BL21 cells were transformed with the pET28a-MSP1D1 plasmid by heat shock. The pET28a-MSP1D1 plasmid contains the genetic sequence for MSP1E3D1, a variant of membrane scaffolding protein (MSP). The Kan^{r-} gene is plasmid-borne on PET28a, allowing transformed cells to grow on YT-Agar media (0.5% (w/v) yeast extract, 0.8% (w/v) tryptone, 85.6 mM NaCl and 0.75% (w/v) agar) containing 25 mg/mL Kanamycin.

Overexpression & Induction of Competent Cells

Cell cultures were grown in YT media (0.5% (w/v) yeast extract, 0.8% (w/v) tryptone, 85.6 mM NaCl, 0.2% (w/v) glucose, and 0.01mg/mL Kanamycin). 5 mL cultures of YT media were inoculated with single colonies of transformed cells and incubated for 2 hours (to an OD of 0.3-0.4) at 37°C and 250 RPM. Cultures that grew the fastest were used to inoculate the four 500 mL cultures of YT media, which were grown for 3.5 hours (to an OD of 0.8 to 1.0) at 37°C and 250 RPM. Once an optimal OD was reached, MSP expression was induced by adding Isopropyl β-D-1-thiogalactopyranoside (IPTG) to a final concentration of 1 mM. Cell cultures expressed MSP for 2.5 hours at 26°C and 250 RPM. Following induction, cells were pelleted by centrifugation at 5,000 RPM for 20 minutes in a Sorvall GSA rotor. The

supernatant was decanted, the pellets flash frozen with liquid nitrogen, and stored at -80°C until needed for purification.

Affinity Purification of Membrane Scaffolding Protein

Pellets were thawed on ice for 15 minutes before being resuspended in Resuspension Buffer (20 mM NaH_2PO_4-H_2O and 1 mM phenylmethanesulfonylfluoride (PMSF), pH 7.5). Triton X-100 was added to the resuspended pellets to a final concentration of 1% (v/v) before cells were disrupted by sonication using a Q700 Qsonica sonicator. Cell samples were placed in ice and sonicated at 50% amplitude for five rounds (1 minute on, 2 minutes off). Lysed cells were centrifuged in a Sorvall SA-600 rotor at 30,000 g for 30 minutes. NaCl was added to the supernatant to a final concentration of 0.3 M before being incubated with Ni-NTA from Quiagen, while rotating at 4°C for half an hour, to allow the affinity tag on MSP to bind to nickel. The Ni-NTA and supernatant slurry was run through a BioRad Polyprep Chromatography Column. The column was washed with increasing concentrations of imidazole (40 mM Tris-HCl, 300 mM NaCl, and 0, 20, 50, or 400 mM imidazole, pH 8.0) with each fraction collected as the flow through, three washes, or six elution fractions respectively. Samples from each fraction were loaded onto a 12.5% SDS-PAGE gel and used to identify peak fractions containing MSP. The peak MSP fractions were the first three elution fractions. Fractions containing MSP were added to a 2,000 MWCO dialysis cassette from Slide-A-Lyzer and dialyzed against 3 L of Dialysis Buffer (20 mM Tris-HCl, 100 mM NaCl and 0.5 mM EDTA, pH 7.4) overnight. The concentration of MSP was determined by an ε_{280} of 29,400 mM^{-1} cm^{-1}.

Purification of Respiratory Complex IV from Isolated Mitochondria

All steps were performed on ice or in the cold room at 4°C. 14 to 16 mg of isolated mitochondria were first thawed on ice for 40 minutes before being sedimented at 14,000 RPM for 5 minutes. The

pellets were resuspended in Resuspension Buffer containing n-Dodecyl β-D-maltoside (DDM) (50 mM 3-(N-morpholino)propanesulfonic acid (MOPS) and 2% (w/v) DDM, pH 8.0) and incubated for 30 minutes to disrupt the mitochondrial membranes. Mitochondrial membrane lipids were pelleted from solution by centrifuging the samples at 14,000 RPM and 4°C for 10 minutes. The imidazole concentration of the supernatant was brought to 5 mM before incubating with Ni-NTA. The mitochondrial suspension was incubated with Ni-NTA agarose for one hour to allow the affinity tag on Cox13 on Complex IV to bind. The incubated solution was run through a BioRad Polyprep Chromatography Column. The mitochondrial components of the solution that did not have affinity for nickel were eluted from the column in the flow through fraction. The column was washed with Wash Buffer (50 mM MOPS, 150 mM NaCl, and 0.009% (w/v) DDM, pH 8.0) with increasing concentrations of imidazole (5 or 10 mM) to wash off any protein that was nonspecifically bound to column and had low affinity for the matrix. Respiratory Complex IV was eluted from the column using Wash Buffer containing increasingly high concentrations of imidazole (100, 200 and 300 mM). All fractions were collected and characterized to identify the peak fractions of Complex IV using a catalytic activity assay.

Assay of Catalytic Activity of Respiratory Complex IV

The redox activity of respiratory Complex IV was quantified colorimetrically by measuring the alteration of absorbance of added cytochrome *c*, which absorbs maximally at 550 nm in the reduced form. Time course measurements were conducted using an Ultrospec 2100 pro UV/Visible Spectrophotometer from Amersham Biosciences, reading the absorbance at 550 nm in 5-second intervals for a total of 180 seconds. The spectrophotometer was blanked with 75 µL of Assay Buffer (50 mM KPO_4 and EDTA, pH 8.0) and 75 µL of the same buffer as the Complex IV sample. The sample used to quantify the enzymatic activity was composed of 75 µL of Assay Buffer, 75 µL of Complex IV sample, and 4 uL of 1700 µM cytochrome *c*, for a final concentration of 45 µM cytochrome *c*. The reaction mixture

was thoroughly mixed by pipetting up and down seven times, taking approximately 10 seconds, before being measured by the spectrophotometer.

Delipidation of Isolated Respiratory Complex IV

Peak fractions of Complex IV were pooled and concentrated in a 3,000 MWCO YM-100 Millipore concentrator to a final volume of 200-300 µL. Delipidation Buffer (50 mM MOPS, 15.8 mM $CaCl_2$, and 20% (v/v) glycerol, pH 7.4) was added to the concentrated Complex IV, for a final volume of 1 mL. 10 uL of Complex IV in Delipidation Buffer was removed for characterization using a Pierce assay and compared to a BSA standard curve to determine the concentration. Porcine phospholipase A2 was added to Complex IV in Delipidation Buffer in ten times molar excess to ensure removal of cardiolipin from Complex IV. Porcine phospholipase A2 has maximal activity against cardiolipin, cleaving it into monolysocardiolipin, which dissociates from Complex IV (29). Work by Sedlak and Robinson (13) has shown that the rate of cardiolipin delipidation is dependent on the detergent solubilizing the protein. Treatment with Triton X-100 results in the highest rate of delipidation (29). For our purposes, Triton X-100 is too harsh a detergent for protein purification and would reduce the stability of Complex IV. Complex IV was treated with porcine phospholipase A2 for 4 hours at room temperature to ensure the cleavage and removal of all endogenous cardiolipin molecules. Porcine phospholipase A2 is calcium dependent and the phospholipase was deactivated by the addition of EDTA to a final concentration of 50 mM. The EDTA was allowed to chelate the calcium in solution for 30 minutes. Following delipidation, an activity assay was performed to ensure Complex IV had not degraded. A 50% decrease in the catalytic activity of Complex IV was observed following removal of cardiolipin (13, 22).

Anion-Exchange Chromatography Purification of Delipidated Complex IV

All steps were performed in a cold room at 4°C. A BioRad Column packed with 2 mL of DEAE Sepharose CL-6B was equilibrated with 200 mL of Equilibration Buffer (50 mM MOPS and 0.015% (w/v) DDM, pH 8.0). Delipidated Complex IV was added to the resin and allowed to flow into the column before being washed with Wash Buffer (50 mM MOPS and 0.01% (w/v) DDM, pH 8.0) containing increasing concentrations of NaCl (50, 100, 150 mM), not depicted in Figure 6. Complex IV was eluted from the column upon washing with Elution Buffer (50 mM MOPS, 0.01% (w/v) DDM, and 500 mM NaCl, pH 8.0). Peak fractions were identified using an Activity Assay before being pooled and concentrated to 500 µL using a 10,000 MWCO YM-100 Millipore concentrator. Porcine phospholipase A2 has a molecular weight of 30 kDa, while Complex IV has a molecular weight of 205 kDa, meaning that any phospholipase remaining in the peak fractions would be eluted, while all of the Complex IV would be retained in the concentrator.

Nanodisc Formation Reaction

Lipid blends were prepared by measuring out and drying down POPC (1-palmitoyl-2-oleoyl-sn-glycero-3-phosphocholine) only or BM (40 mole % POPC, 40 mole % POPE (1-palmitoyl-2-oleoyl-sn-glycero-3-phosphoethanolamine), and 20 mole % tetraoleoyl cardiolipin) lipid blends under a nitrogen stream for 5 minutes each, before being placed in a desiccator for a minimum of 2 hours. Each lipid blend was individually rehydrated in Buffer 2 (20 mM Tris-HCl, 100 mM NaCl, 0.5 mM EDTA, and 59 mM Cholate, pH 7.4) and sonicated in a bath sonicator until all of the lipid film was rehydrated in solution. The nanodisc components (listed below) were allowed to incubate for 30 minutes at 4°C. The BM nanodisc reaction was based on a 143:1 lipid to protein ratio and contained 33 µM BM lipids, 49 µM MSP1E3D1, 250 µL of purified lipid-free Complex IV, as well as 20 mM Tris-HCl, 100 mM NaCl, and 0.05 mM EDTA. The POPC nanodisc reaction was based on a 150:1 lipid to protein ratio and contained 37 µM

BM lipids, 49 µM MSP1E3D1, 250 µL of purified lipid-free Complex IV, as well as 20 mM Tris-HCl, 100 mM NaCl, and 0.08 mM EDTA. Pre-hydrated BioBeads were added to the reaction to remove all detergent and initiate nanodisc formation. Previous studies have shown that BioBeads do not absorb a significant amount of membrane protein (13). Each nanodisc reaction was incubated at 4°C for 9 hours. The nanodiscs were then removed from the BioBeads and incubated with equilibrated Ni-NTA for 45 minutes at 4°C on a rotator. The incubated nickel beads were poured through a BioRad Polyprep column and washed with two column volumes of Wash Buffer (40 mM Tris-HCl and 300 mM NaCl, pH 8.0) containing increasing concentrations of imidazole: 0 mM for Wash 1, 20 mM for Wash 2, 50 mM for Wash 3, and 400 mM for the Elution. Samples from every fraction were run out on a 12% SDS-PAGE gel and stained to determine the location of MSP. Peak fractions were pooled in a 3,000 MWCO Millipore concentrator and washed with around 20 mL of Dialysis Buffer (40 mM Tris-HCl and 300 mM NaCl, pH 7.4) to remove all imidazole from solution. The nanodiscs were concentrated to a final volume of 375 µL.

Complex IV Nanodisc Activity Assay

The enzymatic activity of each of the nanodisc samples was quantified by measuring the redox activity of the protein through the oxidation of cytochrome *c* as described above. This was achieved through time course measurements using a spectrophotometer, reading the absorbance at 550 nm in 5 second intervals for a total of 180 seconds. The spectrophotometer was blanked with 75 µL of Assay Buffer and 75 µL of Dialysis Buffer. Nanodisc samples contained 75 µL of Assay Buffer, 75 µL of Complex IV nanodisc sample, and 27, 32, 37, or 42 µM cytochrome *c*. One control sample for each nanodisc type was incubated with Assay Buffer containing 6 mM KCN. The reaction mixture was thoroughly mixed by pipetting up and down seven times before being measured by the spectrophotometer taking approximately 10 seconds.

Dynamic Light Scattering

The diameter of nanodisc samples was determined using a Zetasizer Helix from Malvern. BM and POPC nanodisc samples were tested to confirm the successful formation of nanodiscs.

Statistical Analysis

A two-tailed student's T-test (unequal variance) was used to determine statistical significance ($p<0.05$) for differences in enzymatic activity.

RESULTS:

Multiple approaches confirm that nanodiscs containing respiratory Complex IV were successfully created. Dynamic Light Scattering showed that nanodiscs of fairly uniform diameter were created and constituted the majority of the BM and POPC nanodisc samples (Figure 7). BM nanodiscs were much more homogenous than the POPC nanodiscs.

An attempt was made to identify endogenous lipids that were co-purifying with Complex IV using TLC. When the endogenous lipids were extracted from purified Complex IV, the concentration of lipids extracted from the protein sample was too low to allow for detection with Molybdenum blue spray reagent (Figure not shown).

The presence of respiratory Complex IV in nanodiscs was confirmed using coomassie staining and Western Blotting (Figure 8). The concentration of respiratory Complex IV in the nanodisc purification fractions was too dilute to be detected by coomassie staining; however, the presence of

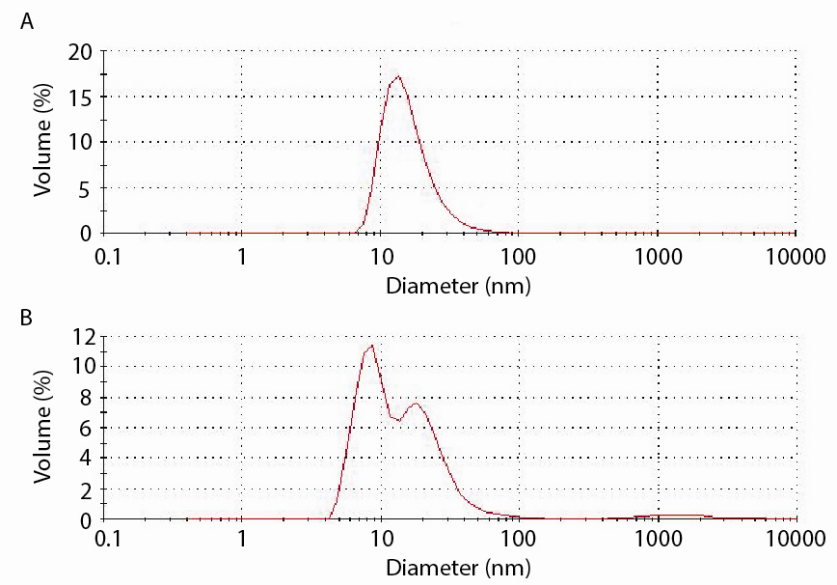

Figure 7 – Dynamic Light Scattering to Determining the Size of Nanodisc Samples
The diameter of particles in concentrated nanodisc samples according to the volume of particles at that size. **A.** The distribution of particle sizes in a concentrated BM nanodisc sample. **B.** The distribution of particle sizes in a concentrated POPC nanodisc sample. The data shown is representative of a single trial.

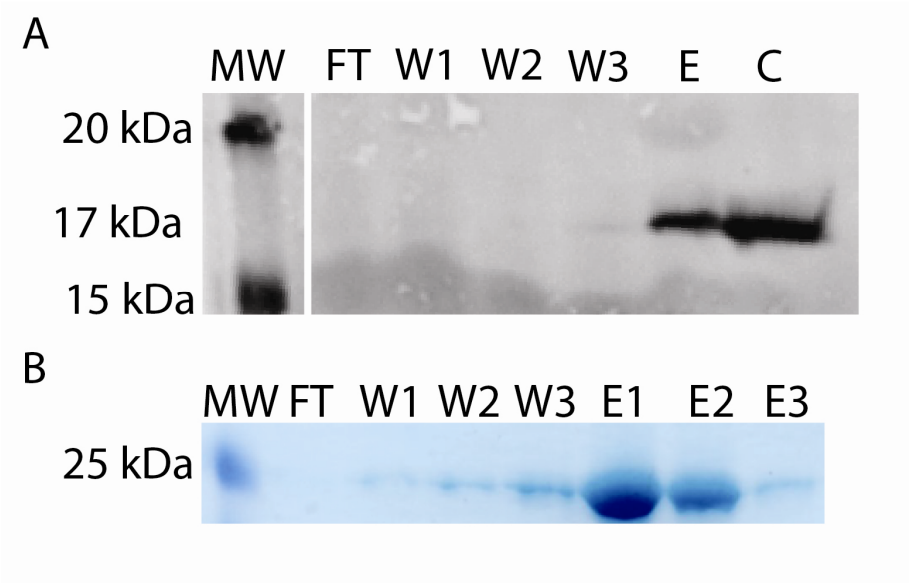

Figure 8 – Elution of Nanodisc Components During Nanodisc Purification
A. The elution of Respiratory Complex IV throughout the course of the nanodisc purification. The presence of Complex IV was determined using anti-Cox4 antibody. Cox4 has a molecular weight of approximately 17 kDa. Key: MW – Molecular Weight Ladder, FT – flow through, W1-W3 – Washes 1 through 3, E – pooled elution fractions, C – control sample of Complex IV. **B.** The elution of MSP throughout the course of nanodisc purification. MSP was detected through coomassie staining. Key: MW – Molecular Weight ladder, W1-W3 – Washes 1 through 3, E1-E3 – Elution fractions 1 through 3. Both gels are representative of all nanodisc trials containing either POPC or BM lipids.

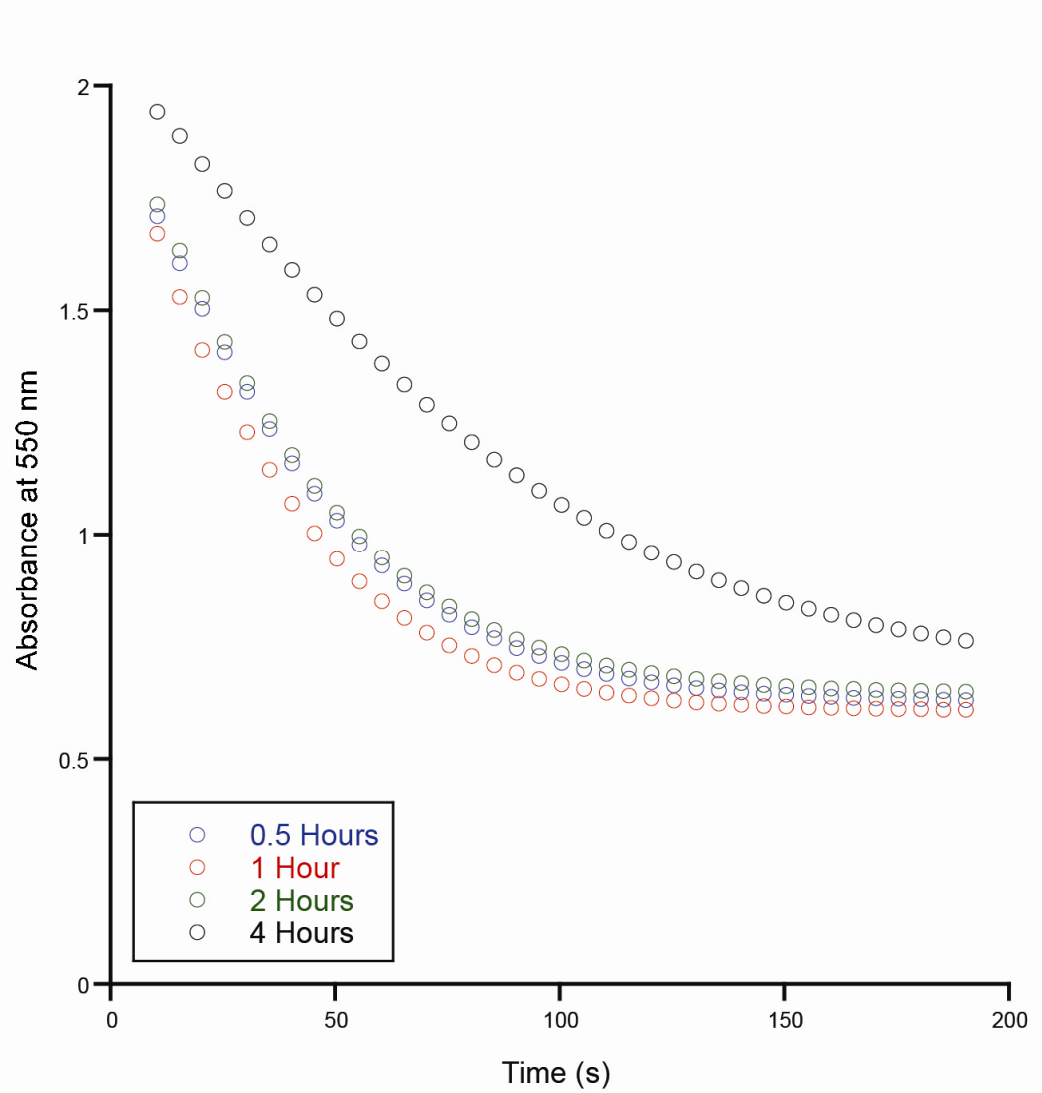

Figure 9 – The Catalytic Activity of Respiratory Complex IV Depending on the Duration of Porcine phospholipase A2 Treatment Detergent solubilized Complex IV samples were treated with porcine phospholipase A2 for between half an hour and four hours before the phospholipase reaction was quenched. The treated Complex IV samples underwent an activity assay with 37 µM cytochrome *c*.

Complex IV was confirmed in nanodisc samples by Western blotting (Figure 8A), silver staining, and SYPRO Orange stain (not shown). The MSP predominantly washes from the affinity column in the first two elution fractions, with relatively small amounts of MSP detaching in every fraction except flow through. Nanodiscs containing respiratory Complex IV appear to detach from the column during the Elution fractions, with a negligible amount of separation occurring during Wash 3.

To find the optimal incubation period to remove endogenous lipids, DDM solubilized respiratory Complex IV was treated with porcine phospholipase A2 for four different periods of time, 0.5 hours, 1

hour, 2 hours and 4 hours. After four hours of incubation, there was a noticeable decrease in the catalytic activity of Complex IV, associated with the removal of endogenous cardiolipin molecules from the protein by phospholipase cleavage of the lipids at the sn-2 position.

The activity of respiratory Complex IV was measured as oxidation of cytochrome *c,* therefore higher activity is observed as a faster decrease in absorbance of reduced cytochrome *c*. Complex IV was found to be more active in nanodiscs containing cardiolipin (BM), than in nanodiscs that did not contain cardiolipin (POPC) (Figure 10). This finding was consistent across all trials, including samples that did not undergo phospholipase treatment. Nanodisc samples pretreated with cyanide displayed a total loss of catalytic activity by Complex IV, confirming that our measured oxidation of cytochrome *c* represented bona fide Complex IV activity.

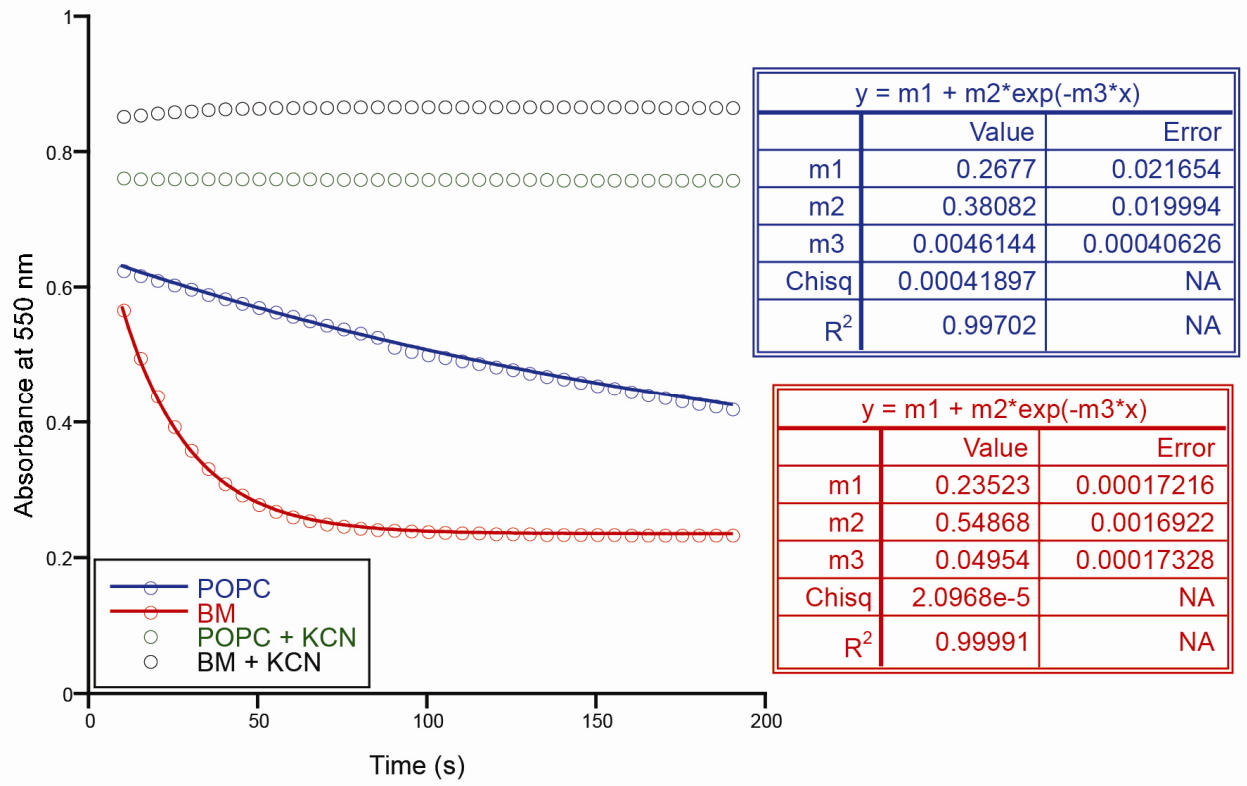

Figure 10 – Characterization of the Enzymatic Activity of Respiratory Complex IV in Differing Lipid Environments
The catalytic activity of Complex IV in nanodiscs containing POPC or a biologically mimetic (BM) lipid blend containing POPC, POPE and cardiolipin. Reduced cytochrome *c* was added to a final concentration of 27 µM to be reduced by Complex IV. Activities were fit according to a first-order exponential decay function. Nanodisc samples were treated with cyanide to inhibit the activity of Complex IV. This graph is representative of three trials.

The oxidation of cytochrome *c* was fit as a first-order exponential decay, with an average R^2 value of 0.9996 and a median R^2 of 0.99991 across all trials. The enzymatic activity can be compared between samples using the first order rate constant (k_1) constant calculated from the line of best fit, seen as m3 in Figure 7. In Table 1, the average *k* values from the line of best fit for each of the lipid blends is displayed. For the BM nanodisc samples, the rate constants ranged from 0.037544 to 0.048653 sec^{-1}, with an average of 0.043019 sec^{-1} across all cytochrome *c* concentrations. The rate of catalysis decreased as the concentration of cytochrome *c* increases. For the POPC nanodisc samples, the average rate constants ranged from 0.003204 to 0.00586 sec^{-1}, with an average of 0.004774 sec^{-1} across all of the cytochrome *c* samples. The rate of catalysis did not appear to have a relationship with the concentration of cytochrome *c*. The difference in the rate of Complex IV catalysis between the BM and POPC nanodiscs was statistically significant ($p<0.05$), and was approximately 10 fold greater in BM nanodisc samples than in POPC nanodisc samples. There was no statistical difference ($p>0.05$) between the POPC nanodisc samples treated with phospholipase and samples that were not. There was a statistical difference ($p<0.05$) between the BM nanodisc samples treated with phospholipase and samples that were not.

	Cytochrome *c* concentration (μM)							
	27		32		37		42	
	k (sec^{-1})	St. Dev.	*k* (sec^{-1})	St. Dev.	*k* (sec^{-1})	St. Dev.	*k* (sec^{-1})	St. Dev.
POPC*	0.005363		0.00586	0.002195	0.003204	0.000286	0.004669	0.001559
POPC - PLA2					0.006142	0.001323		
BM	0.048653	0.005934	0.046346	0.005868	0.039533	0.005009	0.037544	0.008313
BM - PLA2					0.01649	0.000733		

Table 1 – The Average *k* Value Determined from the Line of Best Fit for Complex IV for Nanodisc Samples
k values were averaged for every nanodisc trial. Some of the Complex IV samples (POPC – PLA2 and BM – PLA2) were not treated with phospholipase A2. All values reported for the average of three trials except POPC, determined by the average of two values.

DISCUSSION:

Elution of MSP and Complex IV in the elution fractions (Figure 8) shows that the Complex IV is properly reconstituted in the nanodiscs and that the nanodiscs are purifying as whole units. Work by the

Robinson Group (13, 14) indicates that mammalian subunits COX VIa and VIb dissociate from Complex IV upon the removal of the loosely bound cardiolipin molecules. Given that mammalian COX VIa is homologous to the yeast subunit Cox13, it is reasonable to assume that upon phospholipase treatment, Cox13 would also dissociate. In this experiment, an affinity tag was engineered onto Cox13 to facilitate the purification of Complex IV from yeast, meaning that upon treatment with phospholipase, Cox13 and the affinity tag located on the C-terminus of the subunit would dissociate. MSP also contains an affinity tag to facilitate in the purification of proteins in a model membrane system. The loss of the affinity tag on Complex IV elegantly simplifies the purification of nanodiscs containing Complex IV. Each nanodisc will only contain a single affinity tag. This simplifies the dissociation of the nanodisc from the nickel column because if each nanodisc contained an affinity tag on MSP and Complex IV the dissociation would become much more inconsistent, depending on which affinity tag dissociates first.

MSP1E3D1 nanodiscs have an outer diameter of approximately 12 nm (26). The dynamic light scattering measurements (Figure 7) indicate that BM nanodiscs were created with high homogeneity. Despite the heterogeneity of the POPC nanodiscs, the nanodiscs had an outer diameter of approximately 12 nm, with one population of nanodiscs slightly smaller, one population slightly larger and a large diameter contaminant. These dimensions are consistent with a disc that could accommodate Complex IV. Respiratory complex IV has a cross sectional area of 7.3 nm by 9.3 nm (25), while MSP1E3D1 has an inner diameter of 10.8 nm. This allows Complex IV to exist stably in a nanodisc, surrounded by a 1.5 nm annulus of lipids.

The difference in activity observed between the BM and POPC nanodiscs shows that cardiolipin is playing an important role in the catalytic activity of Complex IV. What was unexpected was the small difference in activity of POPC nanodiscs that did and did not undergo phospholipase treatment. Respiratory Complex IV should retain the tightly bound cardiolipin molecules when not treated with phospholipase, as previous studies have shown that cardiolipin co-purifies with Complex IV (13, 14, 22).

Therefore, Complex IV that does not undergo phospholipase treatment should retain the endogenous cardiolipin molecules and retain high catalytic activity regardless of the lipid environment. Interestingly, when Complex IV was not treated with phospholipase, and was reconstituted into nanodiscs only containing POPC, the nanodisc samples displayed similar activity to Complex IV in nanodiscs that did not contain any endogenous cardiolipin. The activity of the nanodiscs not treated with phospholipase had *k* values that were 10 times lower than the values of Complex IV in a biomimetic lipid blend. This suggests that cardiolipin that is not tightly bound to respiratory Complex IV may play more of a role on the catalytic efficiency than previously believed, and may extend beyond the association of a few endogenous cardiolipin molecules.

Recent research investigating supercomplexes in both bovine and yeast models has discovered that a large number of cardiolipin molecules, 200 in bovine and 50 in yeast supercomplexes, co-purify with the supercomplexes (4). These cardiolipin molecules are too numerous to play a role in the activity of the respiratory complexes acting as annular lipids. These cardiolipin molecules likely co-purify because they are localized in between the respiratory complexes in the supercomplex. This provides some insight into the lipid environment of the respiratory complexes *in vivo*. This knowledge, in conjunction with my findings suggest that cardiolipin molecules also play an important role as bulk lipids, lipids in the membrane surrounding a membrane protein that do not directly interface with the protein, in the inner mitochondrial membrane. The protein-lipid interaction between cardiolipin and Complex IV has never been studied using the nanodisc model membrane system. Previous studies, namely the work by the Robinson Group (13, 14), only investigated the activity in detergent solubilized micelles. Using detergent solubilization, the only lipids remaining attached to the protein were very tightly bound, and for this reason, it is likely that so much emphasis was placed on the tightly bound cardiolipin molecules. While it is likely that the endogenous cardiolipin molecules play a vital role in the

activity of Complex IV, according to my findings the effect of endogenous cardiolipin is overshadowed by the effect of bulk cardiolipin.

Cytochrome *c* is believed to interact with cardiolipin through electrostatic interactions by which the protein associates with the headgroups of cardiolipin (30). Additionally, cardiolipin may insert one or two acyl chains into the hydrophobic pocket of cytochrome *c* to anchor the protein to the lipid bilayer (30). This ability of cardiolipin to interact with cytochrome *c* and recruit the protein to the inner mitochondrial membrane increases the effective concentration of cytochrome *c* at the interfacial region of the bilayer. Increasing the effective concentration of cytochrome *c* may improve the catalytic activity of Complex IV by increasing the availability of cytochrome *c* for oxidation. Cardiolipin could also play a role in the catalytic activity of respiratory Complex IV because of the unique lateral pressure profile that the lipid exerts on the membrane. In high concentrations, cardiolipin will assume a non-lamellar phase characterized by elongated tubes with the headgroups facing the water-filled center of the tube, and the hydrophobic tails facing the outside of the tube. This conformation is known as the hexagonal II phase and is observed in lipids composed of acyl chains containing a greater cross-sectional area than the polar headgroup. This morphology is likely to be partially responsible for the unique structure of the cristae in the inner mitochondrial membrane. The high concentrations of cardiolipin in the inner mitochondrial membrane results in a lateral pressure profile unique to the inner mitochondrial membrane. This unique lateral pressure profile created by cardiolipin could act on respiratory Complex IV, and force the protein to adopt a more active conformation.

Defects in cardiolipin remodeling are associated with Barth syndrome, a disease marked by the enrichment of monolysocardiolipin in the inner mitochondrial membrane (9). Patients suffering from this disease exhibit dysfunction in tissues that have high energetic demands such as the heart and other muscle tissue. This disease underscores the necessity of cardiolipin for proper mitochondrial activity. The experimental findings may have implications into the mechanism by which mitochondrial activity is

decreased by an abundance of monolysocardiolipin. Monolysocardiolipin lacks one of acyl chains that mature cardiolipin has. This could result in a reduced hex II propensity compared when with mature cardiolipin. If Complex IV is squeezed into a more active form by the lateral pressure profile of mature cardiolipin, then deviations from this lateral pressure profile could result in a decrease in the efficiency of Complex IV activity. Monolysocardiolipin contains one less acyl chain than mature cardiolipin. In addition, if cardiolipin inserts one or two acyl chains into the hydrophobic pocket of cytochrome *c* then a decrease in the number of acyl chains could reduce the ability of cytochrome *c* to associate with the membrane, which in turn would reduce the efficiency of Complex IV.

In future experiments these findings can be further investigated using stopped flow absorbance measurements, which would reduce the dead time between the addition of cytochrome *c* to the nanodisc samples and the first reading. A major drawback to this experiment was the uncertainty of the time values recorded. The uncertainty caused variation across all samples, preventing the use of more widely accepted methods of quantifying enzymatic activity. In these experiments, the dead time was approximately 10 seconds. To determine the Michaelis-Menten kinetics of a reaction it will be necessary to know the initial rates of the reaction. With the first 10 seconds of the reaction occurring before the first reading, the initial reaction velocity data was lost. Attempts were made to extrapolate the initial rate of reaction using the line of best fit; however, these data were uncertain and did not fit well enough to allow for the determination of Michaelis-Menten constants. With a stopped flow apparatus, the dead time would be a few milliseconds and the initial reaction velocity could be observed instead of predicted.

Thin layer chromatography was attempted to identify the presence of endogenous cardiolipin molecules. Unfortunately, the cardiolipin molecules were too dilute to detect using molybdenum blue spray reagent. A more sensitive method that can be used to detect endogenous cardiolipin molecules is mass spectrometry. Using this technique, it is possible to detect how many cardiolipin molecules co-

purify with Complex IV. Additionally, mass spectrometry could be used to confirm the removal of the endogenous cardiolipin molecules upon treatment with phospholipase, as well as the dissociation of Cox12 and Cox13 following phospholipase treatment. Having a clear understanding of how many cardiolipin molecules co-purify with Complex IV and what treatment is required to remove the cardiolipin molecules will provide more insight into the protein-lipid interaction. It is important to know that phospholipase treatment is required for the removal of the tightly bound cardiolipin molecules; otherwise, the observed effects of cardiolipin in bulk lipids are not valid. These experiments are currently underway in our group.

Diseases associated with dysfunctional lipid biosynthesis, such as Barth syndrome, can be studied in the future through the creation of nanodiscs using different lipid blends. Nanodiscs enriched in monolysocardiolipin rather than mature cardiolipin could be used to simulate the lipid environment of the inner mitochondrial membrane for an individual suffering from Barth syndrome. Deoxy-cardiolipin, cardiolipin molecule lacking the central hydroxyl group from the linking glycerol, could be used in place of cardiolipin to probe the influence of the endogenous cardiolipin molecules and the function they play as proton antennas for the D-channel.

The mechanism by which the effect of cardiolipin in the bulk lipids can be investigated in future experiments by replacing cytochrome *c* with an electron carrier that does not have the same propensity to interact with lipids. If cardiolipin is recruiting cytochrome *c* to improve the activity of Complex IV then there should be no difference between the catalytic activity of Complex IV in nanodiscs containing cardiolipin and nanodiscs lacking cardiolipin. The effect of the lateral pressure profile of cardiolipin on Complex IV can be elucidated using lipids that display a lateral pressure profile similar to cardiolipin. If cardiolipin was replaced by another lipid, which favors the hexagonal II conformation, then there should be no difference in the catalytic activity of Complex IV if the lateral pressure profile of cardiolipin causes Complex IV to adopt a more catalytically active conformation.

In conclusion, this study has shown that cardiolipin is required for the proper activity of respiratory Complex IV and for the first time suggested a role of cardiolipin in the bulk lipids of the inner mitochondrial membrane for the activity of Complex IV.

References

1. Diaz F. Cytochrome c oxidase deficiency: patients and animal models. Biochim Biophys Acta. 2010 Jan;1802(1):100-10.

2. Schwall CT, Greenwood VL, Alder NN. The stability and activity of respiratory Complex II is cardiolipin-dependent. Biochim Biophys Acta. 2012 Sep;1817(9):1588-96.

3. Pfeiffer K, Gohil V, Stuart RA, Hunte C, Brandt U, Greenberg ML, et al. Cardiolipin stabilizes respiratory chain supercomplexes. J Biol Chem. 2003 Dec 26;278(52):52873-80.

4. Bazan S, Mileykovskaya E, Mallampalli VK, Heacock P, Sparagna GC, Dowhan W. Cardiolipin-dependent reconstitution of respiratory supercomplexes from purified Saccharomyces cerevisiae complexes III and IV. J Biol Chem. 2013 Jan 4;288(1):401-11.

5. Marechal A, Meunier B, Lee D, Orengo C, Rich PR. Yeast cytochrome c oxidase: a model system to study mitochondrial forms of the haem-copper oxidase superfamily. Biochim Biophys Acta. 2012 Apr;1817(4):620-8.

6. Yoshikawa S, Muramoto K, Shinzawa-Itoh K, Mochizuki M. Structural studies on bovine heart cytochrome c oxidase. Biochim Biophys Acta. 2012 Apr;1817(4):579-89.

7. Meunier B, Marechal A, Rich PR. Construction of histidine-tagged yeast mitochondrial cytochrome c oxidase for facile purification of mutant forms. Biochem J. 2012 Jun 1;444(2):199-204.

8. Horvath SE, Daum G. Lipids of mitochondria. Prog Lipid Res. 2013 Oct;52(4):590-614.

9. Claypool SM, Koehler CM. The complexity of cardiolipin in health and disease. Trends Biochem Sci. 2012 Jan;37(1):32-41.

10. Shinzawa-Itoh K, Aoyama H, Muramoto K, Terada H, Kurauchi T, Tadehara Y, et al. Structures and physiological roles of 13 integral lipids of bovine heart cytochrome c oxidase. EMBO J. 2007 Mar 21;26(6):1713-25.

11. Kates M, Syz JY, Gosser D, Haines TH. pH-dissociation characteristics of cardiolipin and its 2'-deoxy analogue. Lipids. 1993 Oct;28(10):877-82.

12. Olofsson G, Sparr E. Ionization constants pKa of cardiolipin. PLoS One. 2013 Sep 13;8(9):e73040.

13. Sedlak E, Robinson NC. Phospholipase A(2) digestion of cardiolipin bound to bovine cytochrome c oxidase alters both activity and quaternary structure. Biochemistry. 1999 Nov 9;38(45):14966-72.

14. Sedlak E, Panda M, Dale MP, Weintraub ST, Robinson NC. Photolabeling of cardiolipin binding subunits within bovine heart cytochrome c oxidase. Biochemistry. 2006 Jan 24;45(3):746-54.

15. Raja V, Greenberg ML. The functions of cardiolipin in cellular metabolism-potential modifiers of the Barth syndrome phenotype. Chem Phys Lipids. 2014 Apr;179:49-56.

16. Tymoczko JL, Berg JM, Stryer L. Biochemistry and the Unity of Life. In: Biochemistry A short Course. 2nd ed. New York, NY: W.H. Freeman and Complany; 2013. p. 3.

17. Barrientos A, Gouget K, Horn D, Soto IC, Fontanesi F. Suppression mechanisms of COX assembly defects in yeast and human: insights into the COX assembly process. Biochim Biophys Acta. 2009 Jan;1793(1):97-107.

18. Poyton RO, McEwen JE. Crosstalk between nuclear and mitochondrial genomes. Annu Rev Biochem. 1996;65:563-607.

19. Paradies G, Paradies V, De Benedictis V, Ruggiero FM, Petrosillo G. Functional role of cardiolipin in mitochondrial bioenergetics. Biochim Biophys Acta. 2014 Apr;1837(4):408-17.

20. Paradies G, Paradies V, Ruggiero FM, Petrosillo G. Cardiolipin and mitochondrial function in health and disease. Antioxid Redox Signal. 2014 Apr 20;20(12):1925-53.

21. Arnarez C, Marrink SJ, Periole X. Identification of cardiolipin binding sites on cytochrome c oxidase at the entrance of proton channels. Sci Rep. 2013;3:1263.

22. Musatov A, Robinson NC. Bound cardiolipin is essential for cytochrome c oxidase proton translocation. Biochimie. 2014 Oct;105:159-64.

23. Buckland AG, Kinkaid AR, Wilton DC. Cardiolipin hydrolysis by human phospholipases A2. The multiple enzymatic activities of human cytosolic phospholipase A2. Biochim Biophys Acta. 1998 Feb 5;1390(1):65-72.

24. Frank V, Kadenbach B. Regulation of the H+/e- stoichiometry of cytochrome c oxidase from bovine heart by intramitochondrial ATP/ADP ratios. FEBS Lett. 1996 Mar 11;382(1-2):121-4.

25. Long AR, O'Brien CC, Malhotra K, Schwall CT, Albert AD, Watts A, et al. A detergent-free strategy for the reconstitution of active enzyme complexes from native biological membranes into nanoscale discs. BMC Biotechnol. 2013 May 11;13:41,6750-13-41.

26. Bayburt TH, Sligar SG. Membrane protein assembly into Nanodiscs. FEBS Lett. 2010 May 3;584(9):1721-7.

27. Nath A, Atkins WM, Sligar SG. Applications of phospholipid bilayer nanodiscs in the study of membranes and membrane proteins. Biochemistry. 2007 Feb 27;46(8):2059-69.

28. Myer YP, Kumar S. Ascorbate reduction of horse heart cytochrome c. A zero-energy reduction reaction. J Biol Chem. 1984 Jul 10;259(13):8144-50.

29. Hsu YH, Dumlao DS, Cao J, Dennis EA. Assessing phospholipase A2 activity toward cardiolipin by mass spectrometry. PLoS One. 2013;8(3):e59267.

30. Muenzner J, Pletneva EV. Structural transformations of cytochrome c upon interaction with cardiolipin. Chem Phys Lipids. 2014 Apr;179:57-63.

31. Sun MG, Williams J, Munoz-Pinedo C, Perkins GA, Brown JM, Ellisman MH, et al. Correlated three-dimensional light and electron microscopy reveals transformation of mitochondria during apoptosis. Nat Cell Biol. 2007 Sep;9(9):1057-65.